Journal of The Electrochemical Society, **157** (6) H589-H592 (2010)
0013-4651/2010/157(6)/H589/4/$28.00 © The Electrochemical Society

Platinum Nanoparticles Grown by Atomic Layer Deposition for Charge Storage Memory Applications

Steven Novak, Bongmook Lee,* Xiangyu Yang, and Veena Misra[z]

Department of Electrical and Computer Engineering, North Carolina State University, Raleigh, North Carolina 27695, USA

This paper explores platinum nanoparticle formation during the early stages of growth by atomic layer deposition. Particle size and distribution can be controlled by altering growth parameters. The particles show excellent temperature stability up to 900°C as examined by transmission electron microscopy and in situ heating. Capacitance–voltage and charge retention measurements demonstrate the memory effect in metal-oxide-semiconductor capacitors with embedded nanoparticles. The size, density, charge storage, and temperature stability of the platinum nanoparticles make them attractive for use as charge storage layers for nonvolatile memory devices.
 [DOI: 10.1149/1.3365031]

Manuscript submitted November 13, 2009; revised manuscript received February 22, 2010. Published April 19, 2010.

As charge storage memory densities increase and device dimensions decrease, there is a need to replace floating polysilicon gates with discrete charge storage materials. Memory technologies utilizing discrete charge storage layers such as silicon nitride, metal nanoparticle, or semiconducting nanoparticles are expected to lessen the impact of localized oxide defects, lateral coupling of charge storage layers between adjacent devices, and stress-induced leakage current.[1,2] Nanoparticle-based memories have reduced lateral conductions over nitride based memories due to the coulomb blockade effect, which is present for nanoscale charged particles.[3] Additionally, metal nanocrystals have higher density of states than semiconducting nanoparticles, allowing higher charge storage densities and faster read/write times.[4] High work function metals, such as Au, Pt, Ni, and Ru, are being looked at for nonvolatile memory applications[5,6] partly because they create additional depth to the potential well formed in between the blocking and inter-polydielectrics, which allows longer retention times in memory devices. Pt and Ru, in particular, show low diffusivities and high thermal stabilities in conventional complementary metal oxide semiconductor processing, making them particularly attractive for charge storage memory technologies.

Achieving long-range uniformity and high densities of nanocrystal growth remains one of the largest hurdles to large-scale manufacturing of nanocrystal memories. Atomic layer deposition (ALD) processes for thin films have the advantage of monolayer growth precision over a large area and the ability to deposit conformally over high aspect ratio features. This uniformity and control over small dimensions of ALD are also attractive for nanoparticle formation for memory applications. Growth of Ru nanocrystals by ALD has been shown previously, but high cycle counts and low densities make this process undesirable for commercial memory applications.[7] A hybrid chemical vapor deposition (CVD)/ALD process has also been used to grow Ru nanocrystals; however, the growth window is very small due to the CVD aspect of crystal growth, and uniformity and densities on SiO_2 are undesirable for memory applications.[8] The recent development of a Pt thin-film ALD process has opened the possibility of adapting it for use in nanocrystal growth.[9] In this study, we have investigated the initial stages of Pt ALD to form nanoparticles that are attractive for nonvolatile charge storage memories. We have explored the role of the starting surface, the ALD deposition conditions, and the top capping layer on the size, density, and stability of Pt nanoparticles.

Experimental

Both SiO_2 and Al_2O_3 dielectrics were grown on (100)-oriented p-type silicon wafers. Dielectrics were either grown thermally in dry O_2 (SiO_2) or deposited by ALD of trimethylaluminum and H_2O (Al_2O_3). Pt was deposited by ALD using (methylcyclopentadienyl) trimethyl-platinum ($MeCpPtMe_3$) and ultrahigh purity O_2. To examine Pt growth, the platinum ALD process was performed on Al_2O_3 and SiO_2 dielectrics with cycles ranging from 5 to 50 cycles in steps of five cycles at 270°C. Unless otherwise stated, the Pt ALD was done with a 0 s exposure time for the Pt precursor. With 0 s exposure, the stop valve between the reaction chamber and the vacuum pump of the ALD tool was continuously opened and pumped. For the ALD samples that received exposure, the stop valve was closed before the precursor was introduced into the chamber, and the precursor was allowed to react with the substrate for a longer period of time.

Physical characterization was done by atomic force microscopy (AFM) and transmission electron microscopy (TEM), and chemical analysis was done by X-ray photoelectron spectroscopy (XPS).

Capacitors were fabricated by thermal oxidation of Si (6 nm) on RCA-cleaned p-type silicon wafers. Pt nanoparticles were grown on the thermal SiO_2 using 35 cycles of the Pt ALD process. Thirty five cycles was chosen as the cycle count where densities and sizes were relatively high, but there was still a window before the films were continuous. HfO_2 was deposited by ALD ($\sim$14.4 nm) to act as the inter-polyoxide. The gate was formed by depositing 90 nm of W in an ultrahigh vacuum radio-frequency sputtering system and patterned into 100×100 μm capacitors by photolithography and wet etching. Samples were annealed for 5 min in 5% H_2/N_2 at 450°C to reduce charges in the dielectric. Capacitance vs voltage (C-V) was measured with an HP4284 LCR, current vs voltage measurements were made with an HP4155b semiconductor parameter analyzer, and the physical parameters were extracted by least-squares curve-fitting using the NCSU CVC program.[10]

Results and Discussion

The ALD process for Pt as well as other noble metals is dependent on the presence of either oxygen or hydrogen as a reactant for the precursor.[9,11] The Pt ALD process used in this study consists of a pulse of O_2 reacting with the surface layer of Pt to create PtO_x. Then, a pulse of $MeCpPtMe_3$ reacts with the PtO_x layer, and during the subsequent purge, O atoms are removed, leaving only Pt. On the next cycle, the O_2 pulse removes any unreacted precursor and oxidizes the Pt surface, preparing it for the next cycle. Previous reports of this mechanism assume a Pt surface to start with, and conformal growth.[9,12] The nucleation of the Pt ALD process, however, is very dependent on the starting surface conditions. The presence of oxygen at the deposition surface determines how Pt nucleates in the ALD process.

In our study, the nucleation and initial growth of Pt were investigated on both SiO_2 and Al_2O_3 as these are potential tunnel dielectrics for memory devices. AFM images (Fig. 1) show that for both dielectrics there is an apparent delay in the nucleation of the Pt film

* Electrochemical Society Student Member.
[z] E-mail: vmisra@ncsu.edu

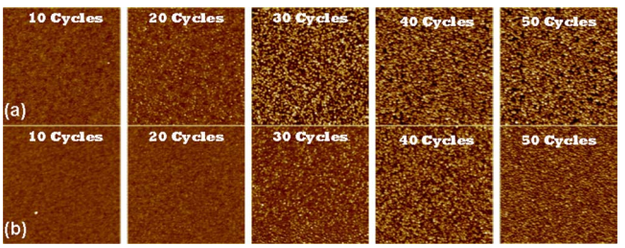

Figure 1. (Color online) AFM image of Pt ALD growth on (a) SiO_2 and (b) Al_2O_3 dielectrics. Particles grow both laterally and vertically with increased ALD cycles. All images are 1 × 1 μm scans with 5 nm *Z*-scale

during the initial cycles. After 20 ALD cycles, the presence of Pt islands can be detected by AFM. The particles are assumed to be spherical, with their radius equal to the *Z* dimension in AFM. Because the size and spacing of the particles are smaller than typical AFM tip widths (7–10 nm), the expected distortion in the *XY* plane is observed. With increased ALD cycles, the particle sizes continue to increase on both dielectrics. As can be seen, the Pt islands on SiO_2 initially grow larger than the islands on Al_2O_3; however, the Pt islands on Al_2O_3 nucleate with a slightly higher density than SiO_2. Although the mechanism causing this difference is still being investigated, it has been reported that the density of hydroxyl bonds on the surface of Al_2O_3 is about 3 times denser than on SiO_2 surfaces.[13,14] Therefore, one would expect that the nucleation density of the Pt ALD process would be greater on an Al_2O_3 surface. At 40 cycles, the particle densities calculated from the AFM images for Pt on Al_2O_3 and SiO_2 are 3.45×10^{11} and 2.5×10^{11} cm^{-2}, respectively. Indeed, the higher density on Al_2O_3 is inline with expectations based on the OH densities of the two dielectrics. In addition, the Al_2O_3 films in this work were grown by ALD of trimethylaluminum and H_2O and, thus, are expected to contain a high density of OH groups.

Root-mean-square (rms) roughness and particle height as obtained from AFM (Fig. 2) indicate that the increase in particle density on Al_2O_3 dielectrics is accompanied by a decrease in particle size and sample roughness as compared to the same cycle number on SiO_2. Therefore, the particles on Al_2O_3 are smaller but have a higher density than the particles on SiO_2. At the 50 cycle mark, the Pt on Al_2O_3 already shows a smoother continuous film, which can be seen both in the AFM images (Fig. 1) and by a reduction in variance in the particle height, while the 50 cycles on SiO_2 show a semidiscrete rougher film. The rms roughness data (Fig. 2a) also show that between 40 and 50 cycles of Pt on Al_2O_3, there is a drop in rms values, further indicating a move from discrete particles to a continuous layer of Pt. The smoother nature of the Pt film on Al_2O_3 is a direct consequence of the higher nucleation density. The particles merge sooner after nucleation, compared to ALD Pt on SiO_2,

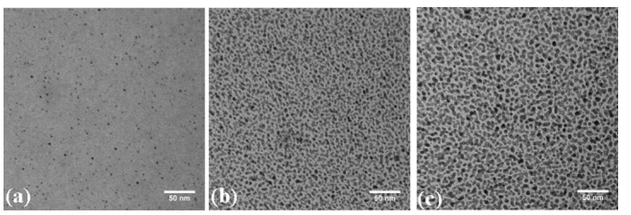

Figure 3. TEM image of Pt nanoparticles grown from 30 cycles Pt ALD on Al_2O_3. With continuous pumping of the ALD precursor, small particle sizes are easily obtained but with a larger spread in size distribution. (b) By allowing the Pt precursor more time to saturate the surface of the dielectric, a larger but more uniform size distribution is obtained. (c) Further increase in precursor exposure leads to minor increases in the particle size. However, the change in size caused by increasing the exposure time from 10 to 20 s is much less than the change seen by increasing the exposure time from 0 to 10 s.

due to their closer proximity and higher density, and require less time to grow vertically before they merge, resulting in a smoother film.

The impact of ALD process parameters on the discontinuous nature of the films and the particle size was further verified by TEM imaging (Fig. 3a). With continuous pumping of the precursor (no exposure time), particle sizes agree with particle height data obtained from AFM images. Increasing the precursor exposure to 10 s results in an increase in the particle size due to the larger reaction time (Fig. 3b). This also indicates that the ALD process with no exposure grows Pt films below the saturated growth regime. Along with the larger particle sizes in the film with exposure, there is also a tighter distribution in the sizes. Further increase in the precursor exposure to 20 s (Fig. 3c) results in a similar particle distribution as the 10 s precursor exposure; a slightly larger particle size is obtained, but the size distributions are very similar. Independent of the precursor exposure, the particle size can be controlled by adjusting the ALD cycle count so that the increase in particle size obtained with an increase in exposure can be countered with reduction in ALD cycles while still maintaining tight particle distributions (Fig. 4).

To ensure that the deposited nanoparticles were indeed metallic, XPS was also performed. A Pt 4f peak located at 71.3 eV[15] with 20 cycles of Pt ALD on Al_2O_3 is clearly observed (Fig. 5), and the intensity of the Pt peak increases with cycle count, indicating an increase in Pt concentration and, hence, in the particle size. The second peak of the Pt 4f doublet is located at 74.23 eV and overlaps with the Al 2p peak at 74.3eV.[15] The increase in the peak height around 74.3 eV is attributed to the increase in the Pt signal, because the growth of any film should shorten the X-ray penetration depth into the Al_2O_3 film and dampen the XPS signal. Similar XPS results

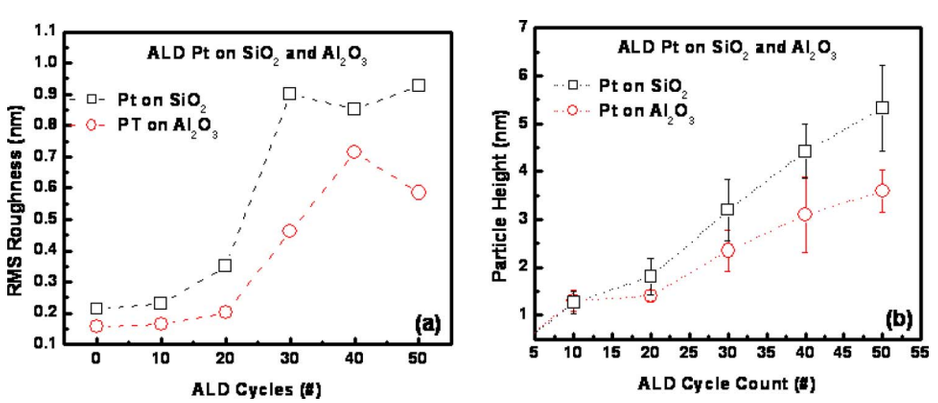

Figure 2. (Color online) (a) RMS roughness data and (b) particle height vs ALD cycle count. The lower rms roughness and particle size can be attributed to a higher nucleation density.

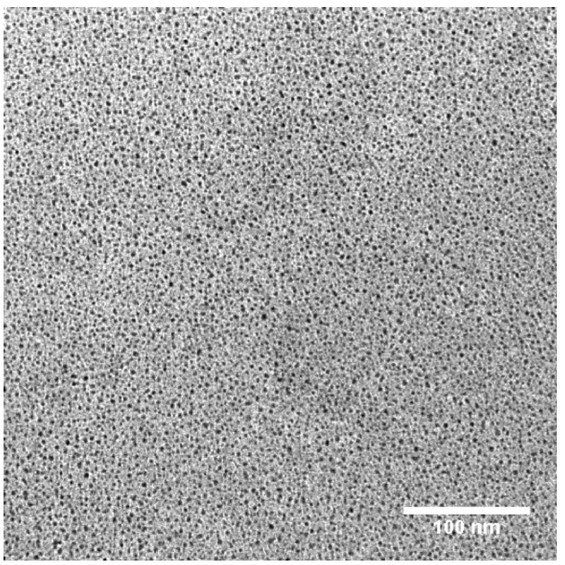

Figure 4. TEM image of 10 cycles of ALD Pt with 10 s precursor exposure. The increase in particle size caused by the precursor exposure is counteracted with the lower cycle count. The result is small, individual particles that are dense and uniformly distributed across the sample.

confirmed the presence of Pt on SiO_2 (not shown). These data suggest that the Pt being deposited is metallic, a key requirement for memory storage.

At higher cycles of Pt ALD, the films become continuous as seen in ALD Pt film literature.[9,16] AFM images of 200 cycles of Pt ALD

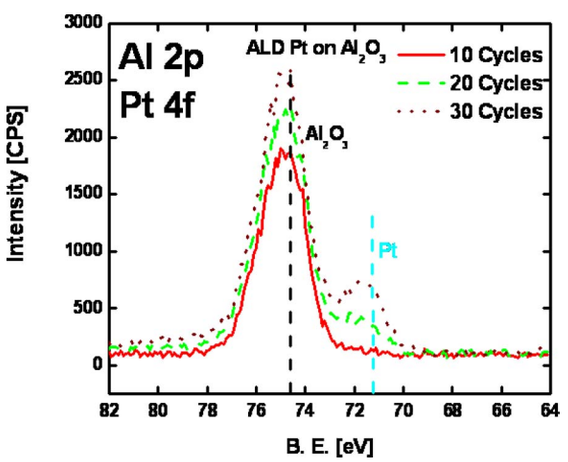

Figure 5. (Color online) XPS data of Pt ALD on Al_2O_3. A detectable Pt signal[16] is present after 20 cycles of ALD matching up with the appearance of particles in AFM. The apparent rise in the Al 2p peak comes from the doublet peak of Pt. Similar XPS behavior is seen for ALD on SiO_2.

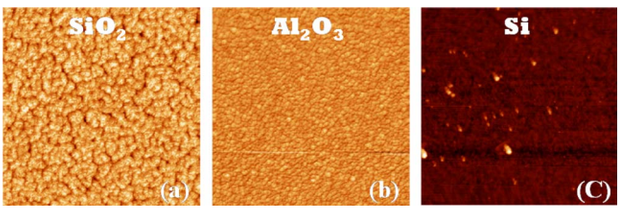

Figure 6. (Color online) 200 Cycles Pt ALD on (a) SiO_2, (b) Al_2O_3, and (C) H-terminated Si. All AFM scans are 1×1 μm with 5 nm *Z*-scale. Pt on SiO_2 shows a folded pattern resembling a brain, while Al_2O_3 shows a smoother film. Relatively small disbursed particles are found on H-terminated Si, indicating lack of Pt nucleation.

on various surfaces (Fig. 6) show the effect of particle nucleations on continuous films. Although both films are continuous on SiO_2 and Al_2O_3, the difference in initial nucleation leads to a different morphology of Pt on SiO_2 compared to Al_2O_3. The less densely nucleated Pt particles on the SiO_2 surface grow until they merge, forming a "brain" pattern with deep channels between the folds. The Pt films, more densely nucleated on the Al_2O_3 surface, merge sooner due to their closer proximity and higher density, resulting in a smoother, more uniform film with smaller grains. An HF last silicon sample was also included in the ALD runs (Fig. 6c). The HF treatment leaves Si–H bonds on the surface of the substrate, which prevents reactions and absorption of the precursor at the samples surface. This inhibits the Pt ALD process from nucleating initially. Repeated exposure to O_2 during ALD cycling eventually creates disbursed Si–OH bonds at the surface, which act as spots to nucleate Pt grains. However, even with 200 cycles, continuous Pt deposition was not achieved on HF last silicon. The large size of the Pt particles on Si (Fig. 6c) indicates that a few Pt particles nucleate in the early cycles and grow with further ALD cycles. With repeated ALD cycling, newer grains start to nucleate, creating relatively smaller particles. To obtain continuous films on HF last Si, much larger number of cycles is necessary. Continuous films have been obtained on HF last Si, but the growth mechanism is still under study. Similar islandlike growth behavior to what we observed on H-terminated Si has been shown for HfO_2 dielectric growth on H-terminated Si.[17]

A cross-sectional schematic of the fabricated test structure is shown in Fig. 6a. Capacitor–voltage data (Fig. 7b) show a large hysteresis effect in metal-oxide-semiconductor (MOS) capacitors embedded with Pt nanoparticles. Pt charging is measured by calculating the flatband (FB) voltage on the forward and reverse sweeps of the hysteresis measurement. At low voltages, there is no significant charging in the Pt layer; however, after about 8 V of applied bias, a large hysteresis is observed. The high voltages coincide with the onset of Fowler–Nordheim tunneling as seen from current–voltage measurements made on the same test structure (not shown), which is desirable for low power memory devices. The charge density was calculated from the change in FB voltage as shown in Eq. 1

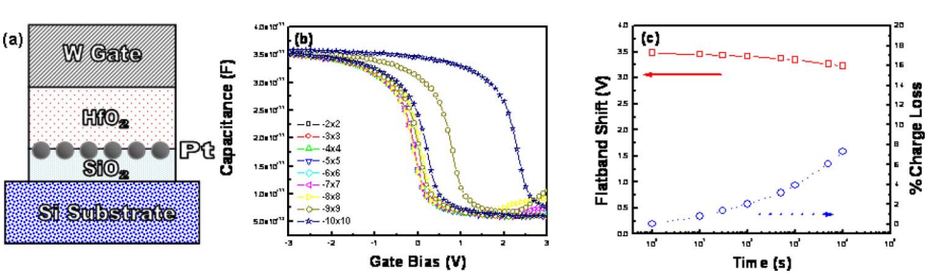

Figure 7. (Color online) (a) CV hysteresis data show charging of Pt nanoparticles. The positive FB shift with positive voltage indicates electron trapping in the nanoparticle layer. Little to no charging is seen for applied voltages less than 8 V, but a large charging effect is seen from FB shifts at higher voltages. (b) Retention data were measured after programming the capacitor at 15 V for 5 s, and the particles show good retention after 10^4 s with less than 8% charge loss.

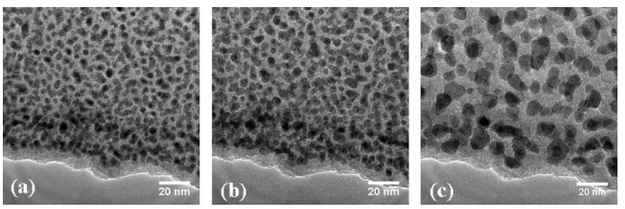

Figure 8. TEM images of Pt particles embedded in Al_2O_3 annealed in situ. (a) As-deposited particles show high density. (b) Almost no change in the particle sizes and structure is seen after annealing up to 900°C for 15 s. (c) After annealing at 1000°C for 5 s, there is a dramatic change in the nanoparticle size and distribution as particles diffuse and coalesce.

$$\Delta N = \frac{C_{\text{G-NP}} \cdot \Delta V_{\text{FB}}}{q} \quad [1]$$

where $C_{\text{G-NP}}$ is the capacitance between the gate and Pt nanoparticles. Peak densities of about 2×10^{13} cm^{-3} are obtained from hysteresis measurements. The FB shift is positive at positive voltages, with respect to the control sample. This indicates the storage of electrons with positive bias, as would be expected for a metal storage layer.

Retention characteristics of the memory capacitors were determined by measuring the FB voltage as a function of time after charging the Pt particles with a 5 s, 15 V voltage pulse (Fig. 7c). The programming pulse gave an initial FB shift of about 3.5 V. After 10^4 s, the FB shift decreased by about 300 mV, which is less than 8% charge loss. These retention characteristics indicate that the high voltages do not significantly degrade the dielectric and, hence, make the use of Pt particle attractive for memory devices.

Temperature stability of the Pt nanoparticles is important for their use in charge storage devices. Floating gate metal-oxide-semiconductor field-effect transistors need to withstand temperatures around 900–1050°C for the source–drain activation anneal. The stability of nanoparticles under temperature is a critical function of the substrate and the capping layer. In this study, the annealing of ALD Pt nanoparticles (20 cycles with 10 s exposure) completely embedded within Al_2O_3 was performed in situ on a custom transmission electron microscope grid provided by Protochips.[18] This grid allows for very rapid changes in temperature within the transmission electron microscope. Negligible change was observed in the size and distribution after annealing at 900°C for 15 s (Fig. 8), indicating that the Pt particles can withstand temperatures needed to activate the source–drain region. However, after further annealing at 1000°C for 5 s, a dramatic change was seen in the particles. The larger size and lower density of particles after 1000°C annealing indicate that Pt nanoparticles underwent (*i*) diffusion through the dielectric and (*ii*) coalescence to create larger particles, which are clearly observable in TEM (Fig. 8c). The effect on electrical characteristics after this change is currently under study and will be reported in a later publication.

Conclusions

In summary, we have demonstrated a process to grow Pt nanoparticles by a low temperature ALD. A process window that utilizes ALD cycle numbers and precursor exposure time to control the particle size was demonstrated. The initial particle density depends heavily on the starting surface. This leaves the possibility of tuning particle density with surface treatments and the ability to change particle size with ALD cycles, both relatively independent of each other. Charging effects are seen for Pt nanoparticles embedded in MOS capacitor structures with high charge densities and good retention characteristics with low charge loss over time. The Pt particles are thermally stable and can withstand source–drain activation anneals of less than 1000°C. However, to allow better device design, further investigation into the electrical behavior and dielectric stability at anneal temperatures at or above 1000°C is needed. Therefore, the high work function, high densities, and good thermal stability of ALD-based Pt nanoparticles are an attractive route for future nonvolatile memory devices and other emerging devices.

Acknowledgments

We thank Protochips for providing transmission electron microscope grids and equipment. This work was supported by the National Science Foundation (NSF ECCS 0802157).

North Carolina State University assisted in meeting the publication costs of this article.

References

1. D. Adams, P. Farfell, M. Jacunski, D. Williams, J. Jakubczak, M. Knoll, and J. Murry, in *Nonvolatile Memory Technology Review*, IEEE, pp. 96–99 (1993).
2. H. I. Hanafi, S. Tiwari, and I. Khan, *IEEE Trans. Electron Devices*, **43**, 1553 (1996).
3. I. Kim, S. Han, K. Han, J. Lee, and H. Shin, *IEEE Electron Device Lett.*, **20**, 630 (1999).
4. Z. Liu, C. Lee, V. Narayanan, G. Pei, and E. C. Kan, *IEEE Trans. Electron Devices*, **49**, 9 (2002).
5. D. Panda, A. Dhar, and S. K. Ray, *Semicond. Sci. Technol.*, **24**, 115020 (2009).
6. P. K. Singh, G. Bisht, R. Hofmann, K. Singh, S. Mahapatra, in *IEEE International Memory Workshop*, IEEE, pp. 1–4 (2009).
7. M. Zhang, W. Chen, S. Ding, X. Wang, D. W. Zhang, and L. Wang, *J. Vac. Sci. Technol. A*, **25**, 775 (2007).
8. D. B. Farmer and R. G. Gordon, *J. Appl. Phys.*, **101**, 124503 (2007).
9. T. Aaltonen, M. Ritala, T. Sajavaara, J. Keinonen, and M. Leskela, *Chem. Mater.*, **15**, 1924 (2003).
10. J. R. Hauser and K. Ahmed, in *Proceedings of the AIP Conference*, AIP, pp. 235–239 (1998).
11. K. J. Park, Ph.D. Thesis, North Carolina State University, Raleigh, NC (2005).
12. T. Aaltonen, A. Rahtu, M. Ritala, and M. Leskela, *Electrochem. Solid-State Lett.*, **6**, C130 (2003).
13. L. T. Zhuravlev, *Langmuir*, **3**, 316 (1987).
14. J. H. Cantrell, *J. Appl. Phys.*, **96**, 3775 (2004).
15. NIST X-ray Photoelectron Spectroscopy Database, Version 3.5, National Institute of Standards and Technology, Gaithersburg (2003) (http://srdata.nist.gov/xps/).
16. Y. Zhu, K. A. Dunn, and A. E. Kaloyeros, *J. Mater. Res.*, **22**, (2007).
17. R. L. Puurunen and W. Vandervorst, *J. Appl. Phys.*, **96**, 7686 (2004).
18. L. F. Allard, W. C. Bigelow, M. Jose-Yacaman, D. P. Nackashi, J. Damiano, and S. E. Mick, *Microsc. Res. Tech.*, **72**, 208 (2009).